BILLIET, Y. & MICHEL, A. (1969). *C. R. Acad. Sci.* **268**, 1129–1131.
BILLIET, Y., SAYARI, A. & ZARROUK, H. (1978). *Acta Cryst.* A**34**, 414–421.
HERMANN, C. (1929). *Z. Kristallogr.* **69**, 533–541.
International Tables for X-ray Crystallography (1952). Vol. I. Birmingham: Kynoch Press.
NEUBÜSER, J. & WONDRATSCHEK, H. (1966). *Liste de Sous-Groupes Maximaux des Groupes Spatiaux.* Communication privée.
SAYARI, A. (1976). Thèse de Spécialité, Tunis (Tunisie).
SAYARI, A. & BILLIET, Y. (1975). *Acta Cryst.* A**31**, S4.
ZARROUK, H. (1976). Thèse de Spécialité, Tunis (Tunisie).
ZARROUK, H. & BILLIET, Y. (1975). *Acta Cryst.* A**31**, S4.

Acta Cryst. (1978). A**34**, 819–823

$X - N$ and Multipole Deformation Electron Density Maps for the Non-centrosymmetric Structure Lithium Formate Monohydrate, $LiHCOO.H_2O$*

BY JOHN O. THOMAS

Institute of Chemistry, University of Uppsala, Box 531, 751 21 *Uppsala, Sweden*

(*Received* 24 *January* 1978; *accepted* 13 *April* 1978)

Room temperature $X - N$ difference electron density maps are calculated for the non-centrosymmetric lithium formate monohydrate, a potential ferroelectric, by taking the phases appropriate to $\mathbf{F}_{o,X}$ as those calculated from a multipole deformation density refinement [Hirshfeld (1971). *Acta Cryst.* B**27**, 769–781]. Both $X - N$ and multipole deformation density maps are presented, and compared with earlier $X - N$ maps derived using less rigorous procedures.

Introduction

The $X - N$ difference electron density ρ_{X-N} at a point $\mathbf{r}$ in the unit cell is given, following the notation of Coppens (1974), by the expression

$$\rho_{X-N}(\mathbf{r}) = \frac{1}{V} \sum_{\mathbf{H}} [k\mathbf{F}_{o,X}(\mathbf{H}) - F_{c,N}(\mathbf{H})] \exp(-2\pi i \mathbf{H} \cdot \mathbf{r}).$$

In an earlier room-temperature determination of the $X - N$ difference density in $LiHCOO.H_2O$ (Thomas, Tellgren & Almlöf, 1975) (hereinafter: TTA), a partial solution was attempted by assigning to $\mathbf{F}_{o,X}$ the phases calculated from a conventional refinement of the X-ray data (using spherical free-atom form factors and individual second-rank thermal vibration tensors). The maps obtained in this way were found to contain more detailed features than those obtained by simply allowing $\mathbf{F}_{o,X}$ to take the phases of $\mathbf{F}_{c,N}$ (see below).

This method is not beyond reproach, however. The use of only spherical free-atom form factors biases the phases calculated from the refinement, since the model takes no explicit account of aspherical stationary charge distributions for the atoms. This inadequacy is here removed, at least in part, by calculating the phases following the refinement of a multipole deformation density function model (Hirshfeld, 1971; Harel & Hirshfeld, 1975).

Calculation of the maps

The multipole deformation density refinement is here made using fixed atomic positional and thermal parameters obtained from the earlier neutron diffraction study (Tellgren, Ramanujam & Liminga, 1974). This is tantamount to expanding the $X - N$ difference density in a basis of deformation density functions centred on the nuclei of the structure (Fig. 1). The deformation model used (Table 1) is described in detail by Hirshfeld (1971). Fixing the neutron-diffraction-determined nuclear positional and thermal parameters eliminates the possibility for correlation effects between bonding and vibrational smearing (Hirshfeld, 1976). It is important that the deformation model should not be constrained in such a way as to impose a significant bias on the calculated phases, and hence on the subsequent appearance of the $X - N$ maps. The latter will clearly still be affected by systematically incorrect positional and thermal parameters from the neutron study, but this is true for centro- and non-centrosymmetric structures alike; it can be combatted only by careful attention to all sources of systematic experimental error, particularly the treatment of extinction.

* Hydrogen Bond Studies. CXXXIII. Part CXXXII: Tegenfeldt, Tellgren, Pedersen & Olovsson (1978). *Acta Cryst.* To be published.

All experimental detail is as described in TTA, but some points associated with the deformation refinement are added here.

(*a*) The $|\mathbf{F}_{o,X}|$ values used as input were previously corrected for extinction (see TTA). No further refinement of extinction was performed.

(*b*) Reflexions with EXT(F) > 1·07 (four in all) were not included, neither were 217 reflexions with $F^2 < 3\sigma(F^2)$, where $\sigma^2(F^2) = \sigma^2_{\text{count}}(F^2) + (0{\cdot}04F^2)^2$.

Table 1. *The multipole deformation density model refined for* $LiHCOO \cdot H_2O$ *after Hirshfeld* (1971)

The *static* deformation density is expressed as

$$\sum_{n,k} c_{nk}\,\varphi_{nk}(r,\theta),$$

where the c_{nk}'s are refinable deformation coefficients. The deformation functions used, φ_{nk}, have the general form

$$N_n r^n \exp(-\gamma r^2)\cos^n\theta_k,$$

where N_n is a normalization factor, n is an integer between 0 and 4, θ_k is the angle between $\mathbf{r}$ and the kth of a chosen set of polar axes, and γ is a parameter governing the breadth of the deformation function. The *dynamical* deformation density is obtained from the static density by applying the refined thermal parameters. The net charge quoted in the right-hand column is the sum of the c_{nk}'s for the k-even terms.

Atom	Point symmetry	Number of deformation density functions	Net charge (e)
Li	spherical	1	+0·77
H	rotation	6	
C	*m*	22	−0·66
O(1)	*m*	22	
O(2)	*m*	22	
O(*W*)	1	35	
H(1)	rotation	6	−0·11
H(2)	rotation	6	
		Total: 120	

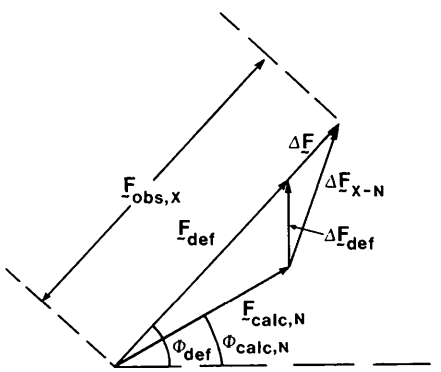

Fig. 1. Diagram illustrating the relation between the dynamic vectors $\mathbf{F}_{o,X}$, $\mathbf{F}_{c,N}$, $\mathbf{F}_{\text{def}}$, $\Delta\mathbf{F}_{X-N}$, $\Delta\mathbf{F}_{\text{def}}$ and $\Delta\mathbf{F}$ ($\mathbf{F}_{o,X} - \mathbf{F}_{c,X}$ residue) for the special situation when the total deformed structure factor $\mathbf{F}_{\text{def}}$ is taken to be the sum of $\mathbf{F}_{c,N}$ and the deformation vector $\Delta\mathbf{F}_{\text{def}}$.

(*c*) Fixed nuclear positional and thermal parameters were taken from Tellgren, Ramanujam & Liminga (1974), free-atom form factors for Li^+, H, C and O were described in TTA.

(*d*) The refined deformation model is summarized in Table 1. Note that no constraints were applied to the deformation functions associated with the water O atom, whereas only a spherical deformation term was refined for Li^+. The start value for the deformation coefficient of Li^+ was 1·0, all other start values were zero. The refined structural model was thus neutral from the outset, and constrained to remain so throughout.

(*e*) Final agreement factors (defined in the usual way) after the deformation refinement were $R(F^2) = 0{\cdot}027$ and $R_w(F^2) = 0{\cdot}071$. The final $R(F)$ value in TTA was 0·033, where only data with $F^2 < 2\sigma(F^2)$ were removed and extinction-affected reflexions were not rejected.

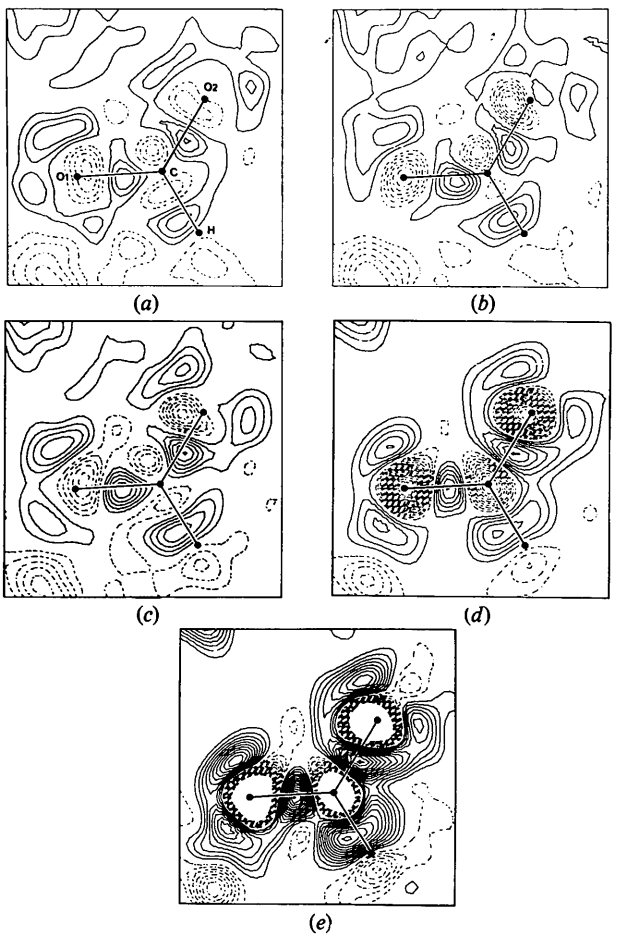

Fig. 2. (*a*)–(*c*) $X - N$ difference density maps (*d*) dynamic and (*e*) static deformation density maps for the $HCOO^-$ ion in $LiHCOO.H_2O$. Maps (*a*) and (*b*) were calculated as described in TTA. All contour intervals 0·05 e Å^{-3}. Zero contour omitted.

(*f*) After four cycles of refinement no shifts were $>0{\cdot}1\sigma$.

The resulting $X - N$ maps for the $HCOO^-$ ion and the H_2O molecule are given in Figs. 2 and 3 along with earlier maps for comparison. The static and dynamic deformation density maps are also included for comparison.

The magnitudes of the mean phase differences $\overline{|\Delta\varphi|}$ between $\mathbf{F}_{o,X}$ and $\mathbf{F}_{c,N}$ for different $|\mathbf{F}|$ ranges are given in Table 2 for both the earlier (TTA) and the present approach. These differences are also analysed in Fig. 4, which shows that $\overline{|\Delta\varphi|}$ values for weaker reflexions are systematically smaller from the present method; this difference disappears for higher $|\mathbf{F}_{o,X}|$ values. Note that *hk*0-type reflexions, for which $\Delta\varphi$ is identically zero, are not considered in this analysis. It is not clear whether the trend seen here for small $|\mathbf{F}|$'s is in any way general; it could, for example, be an artefact of the one-electron deficient model used to calculate $\mathbf{F}_{c,N}$.

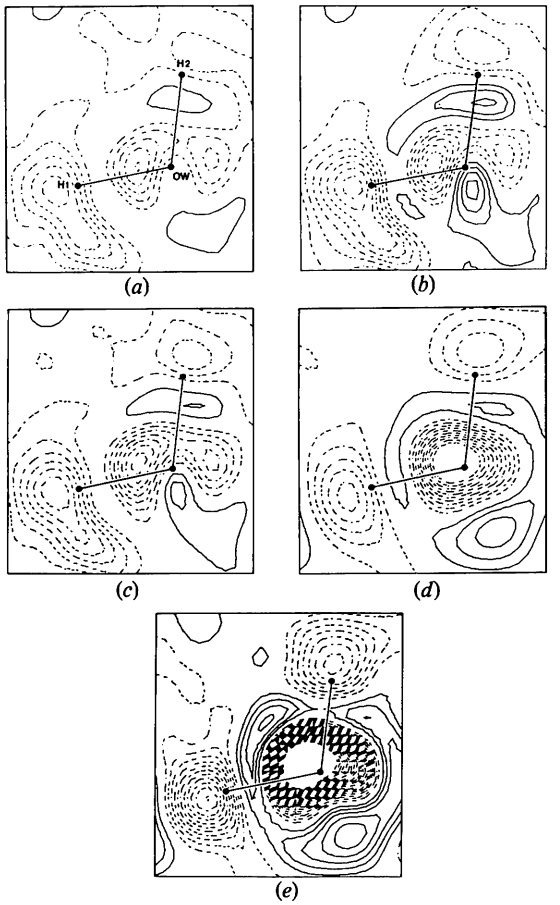

Fig. 3. (*a*)–(*c*) $X - N$ difference density maps, (*d*) dynamic and (*e*) static deformation density maps for the H_2O molecule in $LiHCOO.H_2O$. Maps (*a*) and (*b*) were calculated as described in TTA. All contour intervals 0·05 e Å^{-3}. Zero contours omitted.

Discussion

Any attempt to obtain an $X - N$ deformation density map for a non-centrosymmetric structure must, of necessity, be approximate. The problem is to assess the extent to which these approximations yield meaningful maps.

A reasonable requirement for the correctness of phases calculated from the deformation refinement is that the resulting X-ray difference Fourier map be essentially featureless (Coppens, 1974). Two such syntheses (Fig. 5*b*,*d*) are compared with the corresponding difference syntheses after conventional X-ray refinement (Fig. 5*a*,*c*). Although the difference map for $HCOO^-$ is considerably 'cleaner' after deformation refinement (*cf.* Fig. 5*a* and *b*) the corresponding situation for the H_2O maps is not so encouraging. Systematic features remain in the maps even after the deformation refinement (*cf.* Fig. 5*c* and *d*). There is no obvious explanation for this difference. It is unlikely that some inadequacy in the thermal model (*e.g.* neglect of anharmonicity) could result in such a large effect.

Table 2. *The mean phase difference* (°) *between* $\mathbf{F}_{o,X}$ *and* $\mathbf{F}_{c,N}$ *as calculated in TTA* ($\overline{|\Delta\varphi_1|}$) *and in the present approach* ($\overline{|\Delta\varphi_2|}$) *for different* $|\mathbf{F}|$ *ranges*

N is the number of reflexions in a given range.

$\lvert\mathbf{F}\rvert$ range	$\overline{\lvert\Delta\varphi_1\rvert}$	$\overline{\lvert\Delta\varphi_2\rvert}$	N
0·75–2*	3·33	1·50	343
2–4	2·18	1·38	181
4–6	1·63	1·79	57
6–8	1·11	1·13	40
8–10	1·13	1·19	22
10–12	0·71	0·66	11

* Reflexions with $0 < |\mathbf{F}| \lesssim 0{\cdot}75$ removed

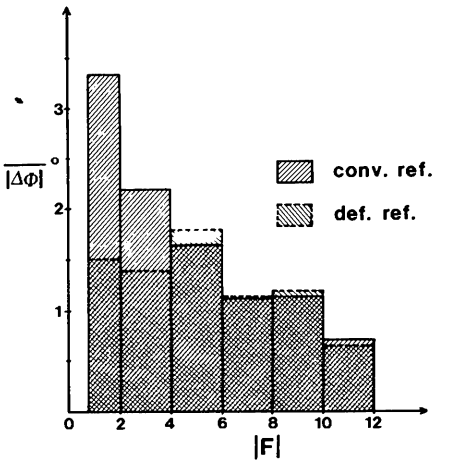

Fig. 4. Mean phase difference between $\mathbf{F}_{c,X}$ and $\mathbf{F}_{c,N}$ for different ranges of $|\mathbf{F}|$ and different methods of calculating $\mathbf{F}_{c,X}$.

It may be noted that, for the deformation model used here, with $\mathbf{F}_{def} = \mathbf{F}_{c,N} + \Delta\mathbf{F}_{def}$ (Fig. 1), the $X - N$ map [*e.g.* Fig. 2(*c*) for $HCOO^-$] should simply be the sum of the dynamic deformation map (Fig. 2*d*) and the residue map (Fig. 5*b*). That this is not exactly true (even for regions some distance away from the atom centres) is because $\mathbf{F}_{c,N}$ has been evaluated for a non-neutral asymmetric unit (Li^+, HCOO and H_2O), with $\Delta\mathbf{F}_{def}$ accounting for the remaining electron. $\mathbf{F}_{o,X}$ has, however, been scaled to $\mathbf{F}_{c,N}$ in the subsequent calculation of the $X - N$ maps.

It follows, therefore, that the $X - N$ map exhibits good quantitative agreement with the thermally smeared deformation density map for the $HCOO^-$ ion (Fig. 2*c* and *d*), while the maps for the water molecule differ significantly (Fig. 3*c* and *d*).

The large negative regions in the refined deformation density maps in the vicinity of atom centres have no physical significance. These are artefacts of the behaviour of the radial functions as r approaches zero.

The $HCOO^-$ *ion*

It is encouraging that the static deformation density maxima in the C—O bonds (Fig. 2*e*) are virtually identical (0·70 e $Å^{-3}$). This would be expected on chemical grounds and was indeed also found in the earlier study (Fig. 2*b*). It can be noted that the maxima in these bond densities are insignificantly higher in the new (dynamic) $X - N$ maps than in the earlier maps (*cf.* Fig. 2 *c* and *b*). The maximum associated with the C—H bond is similarly unchanged. On the other hand, we see that the lone-pair features in the new maps are considerably more distinct. It is of interest to examine these in detail in the light of trends noted recently (Thomas, 1977) in the lone-pair regions of the hydrogen-bonded system $(CH_3)_2NH_2HC_2O_4$. The lone-pair maxima in the static deformation density map (Fig. 2*e*) are ~0·52 and ~0·40 e $Å^{-3}$ for O(1) and ~0·42 and ~0·30 e $Å^{-3}$ for O(2). In the case of O(1), the difference is accompanied by different acceptance situations. The weaker peak lies in the direction of acceptance of the strongest hydrogen bond in the structure [H(1) ... O distance 1·742 (3) Å] (see TTA). The other peak corresponds to a Li—O contact of 1·941 (5) Å. For O(2) the two peaks lie roughly along Li—O contacts of 1·964 (4) and 1·927 (5) Å respectively. In both cases, the apparently weaker electrostatic interaction corresponds to the stronger lone-pair peak. Neither of these effects in the maps is more than marginally significant, however.

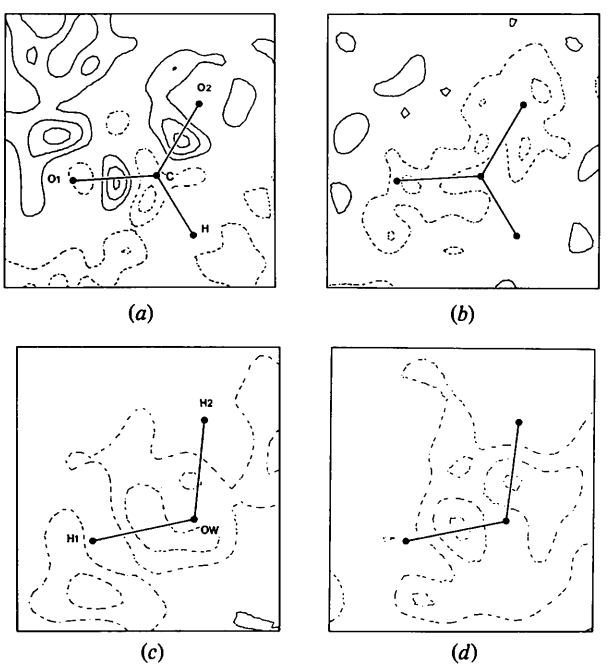

Fig. 5. ($\mathbf{F}_o - \mathbf{F}_c$) difference density maps following the conventional refinement (*a* and *c*) and the deformation refinement (*b* and *d*). Contour intervals 0·05 e $Å^{-3}$. Zero contour omitted.

The H_2O *molecule*

The systematic character of the content of Fig. 5(*d*) encourages little confidence in the meaningfulness of the new difference density maps for the water molecule (Fig. 3*c–e*). The differences noted earlier between the regions of H(1) and H(2) (Fig. 3*b*) and also found in a recent reinvestigation by Harkema, de With & Keute (1977), have all but disappeared as a result of the present treatment. The only feature remaining is the well-developed oxygen lone-pair density in the defor mation density maps (Fig. 3*d* and *e*). The discrepancy between this feature and the appearance of the $X - N$ map (Fig. 3*c*) nevertheless remains unexplained.

X–N maps *versus* deformation density refinement

In the light of the above, it is natural to question the value of calculating an $X - N$ map, especially in the case of a non-centrosymmetric structure. The following advantages of a refinement procedure are clear.

(i) First (and most obvious), a refinement is insensitive to whether or not the structure is centrosymmetric.

(ii) The mathematical model for the difference density can be used directly to obtain other physical quantities, *e.g.* effective atomic charge (and hence charge transfer), dipole moment, electrostatic potential, *etc.*

(iii) The need for neutron data is reduced in as much as the refinement procedure can, in principle, distinguish the effects of bonding and thermal motion

(Hirshfeld, 1976). Neutron data are highly desirable when hydrogen atoms are present, however; but note Stevens & Hope (1975).

(iv) Series-termination effects do not arise in a refinement approach.

(v) There is no 'noise' as such in the resulting deformation maps.

(vi) A deformation refinement should give an essentially correct scale factor.

(vii) An estimate of the error in the refined deformation density is readily obtainable.

An $X - N$ map, at least for a centrosymmetric structure, can nevertheless serve the useful purpose of representing the difference density unbiased by functions chosen to describe the deformation. It can thus be used to assess appropriate constraints for a subsequent deformation model refinement.

I thank Professor Fred Hirshfeld of the Weizmann Institute, Rehovot, Israel for making his program available and for generous assistance with its implementation in Uppsala. I am also greatly indebted to Professor Ivar Olovsson for his active interest and support. This work has been financed by grants from the Swedish Natural Science Research Council.

References

COPPENS, P. (1974). *Acta Cryst.* B**30**, 255–261.
HAREL, M. & HIRSHFELD, F. L. (1975). *Acta Cryst.* B**31**, 162–172.
HARKEMA, S., DE WITH, G. & KEUTE, J. C. (1977). *Acta Cryst.* B**33**, 3971–3973.
HIRSHFELD, F. L. (1971). *Acta Cryst.* B**27**, 769–781.
HIRSHFELD, F. L. (1976). *Acta Cryst.* A**32**, 239–244.
STEVENS, E. D. & HOPE, H. (1975). *Acta Cryst.* A**31**, 494–498.
TELLGREN, R., RAMANUJAM, P. S. & LIMINGA, R. (1974). *Ferroelectrics*, **6**, 191–196.
THOMAS, J. O. (1977). *Acta Cryst.* B**33**, 2867–2876.
THOMAS, J. O., TELLGREN, R. & ALMLÖF. J. (1975). *Acta Cryst.* B**31**, 1946–1955.

SHORT COMMUNICATIONS

Contributions intended for publication under this heading should be expressly so marked; they should not exceed about 1000 *words; they should be forwarded in the usual way to the appropriate Co-editor; they will be published as speedily as possible.*

Acta Cryst. (1978). A**34**, 823–824

Convergence of Brillouin zone summations.

By PETER A. KROON and AAFJE VOS, *Laboratorium voor Structuurchemie, Rijksuniversiteit Groningen, Nijenborgh* 16, 9747 *AG Groningen, The Netherlands*

(*Received* 31 *January* 1978; *accepted* 21 *February* 1978)

A simple method to overcome convergence problems in Brillouin zone summations of lattice dynamical properties is proposed, which makes use of evenly spread sample points and gives a special treatment to points close to the Brillouin zone origin.

Calculation of **T**, **L** and **S** tensors and thermal diffuse scattering involves integration over the Brillouin zone (BZ), or part of it, of functions which are quadratic in the vibration amplitudes **u**. For the acoustic modes σ with small wave vector **k**, the **u** values vary according to

$$\mathbf{u}(\sigma\mathbf{k}) = D(\sigma\hat{\mathbf{k}})/\mathbf{k}, \tag{1}$$

where $D(\sigma\hat{\mathbf{k}})$ is a function smoothly varying with $\hat{\mathbf{k}}$, and $\hat{\mathbf{k}}$ is a unit vector in the direction of **k**. Because

$$\lim_{\mathbf{k}\to 0} u^2(\sigma\mathbf{k}) = \infty \tag{2}$$

difficulties arise if the integration is to be done numerically since the contribution $I(v_0)$ of the volume element v_0 around $\mathbf{k} = 0$ cannot be obtained as $u^2(\sigma,\mathbf{k} = 0)\,v_0$. An estimate of this contribution can be obtained by analytical integration of (1). For a cone around **k** with opening angle $\mathrm{d}\psi$ and its apex coinciding with $\mathbf{k} = 0$ the integrated value is given by

$$I(\mathbf{k}) = D(\sigma\hat{\mathbf{k}})\,k_{\max}\,\mathrm{d}\psi, \tag{3}$$

where $k_{\max}$ is the height of the cone. From this it can be seen that for numerical integrations extremely dense sampling around $\mathbf{k} = 0$ is required to make $I(v_0)$ negligibly small with respect to the contributions of the remaining volume elements, since $I(v_0)$ does not approach zero with v_0 (or $k^3_{\max}$) but with $k_{\max}$. Filippini, Gramaccioli, Simonetta & Suffritti (1976) proposed a method to overcome the convergence problem which is based on a non-isometric sampling grid with dense sampling around $\mathbf{k} = 0$. We have tested their method by calculating the integral of a simple k^{-2} function, but have not achieved the improvement in convergence claimed in their paper. Moreover, sampling methods which make use of unevenly distributed grid points require more programming effort and can become quite cumbersome in, for instance, the double BZ summations occurring in the expressions for the second-order thermal diffuse scattering (Kroon & Vos, 1978*a*).

Since the convergence problem is caused by the behaviour of the acoustic lattice vibrations close to $\mathbf{k} = 0$, and the shape